TÜBİTAK

Turkish Journal of Physics

http://journals.tubitak.gov.tr/physics/

Research Article

Turk J Phys
(2019) 43: 576 – 581
© TÜBİTAK
doi:10.3906/fiz-1905-4

Chemical synthesis of zinc oxide nanorods and their transformation into nanotubes

Pijus Kanti SAMANTA*
Department of Physics (UG & PG), Prabhat Kumar College, Contai, West Bengal, India

Received: 06.05.2019 • **Accepted/Published Online:** 11.09.2019 • **Final Version:** 05.12.2019

Abstract: A simple wet chemical method was successfully deployed to synthesize zinc oxide nanorods and nanotubes of hexagonal morphology. Energy dispersive X-ray spectroscopy confirmed the formation of ZnO with almost equal atomic percentages of Zn and O atoms. The FESEM images confirmed the formation of ZnO nanorods and nanotubes of length 1.5 to 2 μm and diameter 500 nm to 1 μm. The growth of the nanorods saturated under the combined effect of ionic association of Zn^{2+} and OH^- ions, Gibbs' energy of the reaction, reaction temperature, and the enthalpy of the system. Further stirring led to dissolution resulting in coarse edges on the top of the nanorods and finally hollow nanotubes were formed. The synthesized ZnO nanotubes exhibited strong photoluminescence at 649 nm owing to the holes trapped at V_O^{++} states and the conduction band edge.

Key words: Nanoparticles, crystal growth, luminescence, spectroscopy

1. Introduction

Recent research has focused on investigation of the optoelectronic and magnetic properties of nanostructured materials because of their interesting properties compared to the bulk structure. Semiconductor metal-oxide nanostructures are very promising in this context due to their size dependent bandgap tunability. Moreover, their unique electronic properties lead to their application in fabricating LEDs, lasers, optical detectors, gas and chemical sensors, and even biomedical devices [1–3]. Zinc oxide (ZnO) is a very popular semiconductor having a high bandgap of 3.37 eV and excitonic binding energy of 60 meV at room temperature. ZnO has high optical transparency in the visible window [4] and high electrical conductivity. These two properties together make ZnO a potential material for transparent electrodes in solar cells [5]. The high bandgap of ZnO has made it a UV-emitting semiconductor. However, visible emission is also possible by incorporation of several defects and doping of foreign elements [6,7]. ZnO crystallizes in wurtzite structures with a lack of symmetry. Hence the ZnO crystal is polar in nature and is responsible for the piezoelectric property exhibited by it. Piezoelectric energy generation from ZnO nanorods has been demonstrated by Wang et al. [3].

Nanostructures can be fabricated using a variety of methods like chemical, sol-gel, vapor–liquid–solid, sputtering (dc and ac), and physical and chemical evaporation methods [8,9]. However, the chemical bath deposition method is a very simple liquid phase growth method for growing metal oxide nanostructures. The method is very cost effective and the growth parameters can be easily controlled as compared to gas phase growth processes. Tubular nanostructures are of special interest due to their potential applications in gas sensors due to their large surface area. The most commonly adopted methods for synthesizing tubular ZnO nanostructures

*Correspondence: pijush.samanta@gmail.com

are thermal evaporation, the vapor–liquid–solid method, molecular beam epitaxy, electrochemical deposition, the solution method, and the microwave synthesis method. However, most of these processes involve the maintenance of high temperature, low pressure, and flow of carrier gas. In some cases, surfactants are also required. We report here a simple chemical bath deposition method to grow hollow tubular ZnO nanostructures followed by rigorous structural characterization for understanding the underlying structure–property relationship.

2. Materials and methods

All the reagents used in our experiment were of analytical grade and used as supplied by Merck (99.99% pure). First, 2.195 g of zinc acetate dihydrate was dissolved in deionized water to prepare 1 M concentration. Then 1 M NaOH solution was prepared by dissolving 2 g of NaOH in deionized water. The two solutions were mixed under constant stirring for 2 h at room temperature. At the end of the reaction, the white precipitate was filtered and washed with deionized water and methanol consecutively for removal of unreacted salts if present. Then the precipitate was dried in a furnace at 100 °C for further characterization.

Field emission scanning electron microscope (FESEM) data were obtained in a ZEISS FESEM operating at 5 kV to analyze the surface morphology of the synthesized material. Energy dispersive X-ray (EDX) spectroscopic data were collected in situ with the FESEM to study the compositional analysis of the material. The room temperature photoluminescence (PL) spectrum was recorded in a PerkinElmer LS-55 spectrophotometer.

3. Results and discussion

The composition of the synthesized material was investigated using EDX spectroscopy in situ with a FESEM as shown in Figure 1a. It was observed that the material is composed of Zn and O atoms with weight ratio 79.86:20.14 and atomic ratio 49.24:50.76. Typical FESEM images of the synthesized ZnO are shown in Figures 1b and 1c. Well-grown ZnO nanorods and nanotubes were found to have formed. The length of the nanorods and nanotubes varied from $\sim$1.5 to 2 μm and diameter varied from $\sim$500 nm to 1 μm.

To understand the growth of such structures, we have to understand the wurtzite structure of ZnO and the basic reaction mechanism involved in the chemical process. Wurtzite is thermodynamically the most stable and favorable structural configuration of ZnO. The structure can be described as the stacking of Zn^{2+} and O^{2-} ions alternatively along the c-axis (001) of the hexagon. Zn^{2+} and O^{2-} ions in the wurtzite cell are fourfold coordinated and bound via covalent sp^3 bonding. The lattice parameters for such wurtzite structures are $a = 3.249$ and $c = 5.207$ belonging to the space group $P_{63}mc$. The structure exhibits a polar nature along the c-axis of the crystal, one face terminated with the Zn^{2+} ion and the other terminated by the O^{2-} ion. This is a very commonly observed configuration in most grown rod-like ZnO nanostructures. The existing dipole moment along the c-axis leads to bulk truncation due to the divergence of the Madelung energy to these surfaces. Hence these bulk truncated surfaces are not stable. Instead of that, the [0001] and $[\bar{1}]$ polar facets are the most commonly exposed orientation of ZnO crystals. These unstable polar surfaces require more positive or negative charges for their stability and hence the structure stabilizes by reduction of the electrostatic Madelung energy [10,11].

Under constant stirring of the solution, zinc acetate is decomposed into $Zn(OH)_2$, which further decomposes into Zn^{2+} and OH^- in the presence of H_2O. Similarly NaOH is also decomposed to Na^+ and OH^- ions. Finally $Zn(OH)_4^{2-}$ is formed. At the onset of saturation ZnO nuclei are formed. The basic chemical reaction

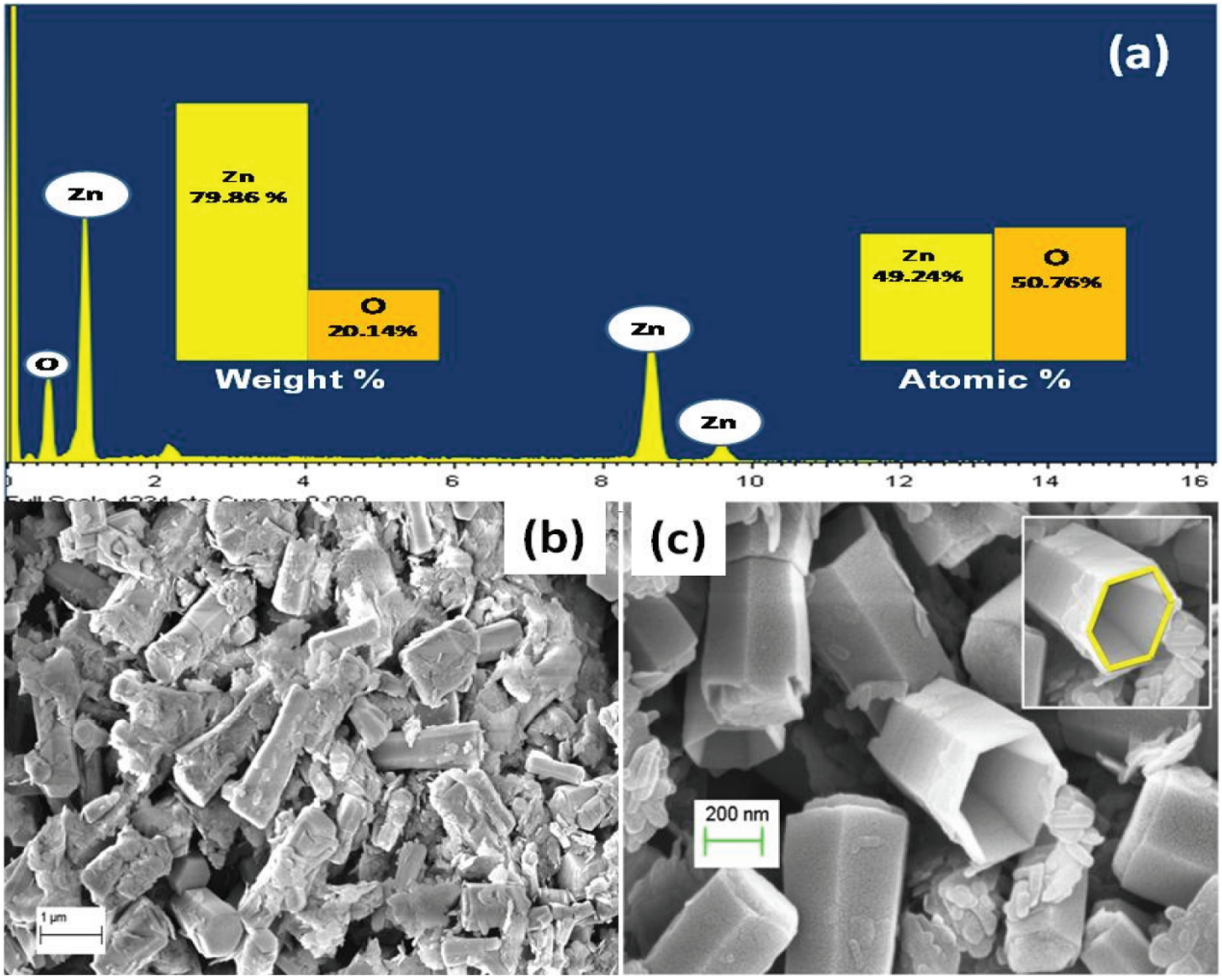

Figure 1. (a) EDX spectrum of synthesized ZnO. The bar diagram in the inset shows the weight and atomic % of Zn and O atoms in the synthesized material; (b, c) FESEM images of the synthesized ZnO nanorods and nanotubes. Inset shows the hexagonal surface morphology of the nanotubes.

involved in the synthesis process is shown below.

$$Zn(CH_3(COO))_2H_2O + NaOH \rightarrow ZnO + 2CH_3(COO)Na + 3H_2O \quad (1)$$

The Gibbs free energy can be calculated using the equation

$$\Delta G_{reaction} = \Delta G_{products} - \Delta G_{reactants} \quad (2)$$

The free energies of different precursors in their respective states are shown in the Table to calculate the favorable direction of growth [12]. Using the above data the free energy of the reaction was calculated to be –938.7 kJ/mol. The decrease in the free energy in the forward direction of the reaction indicates that the forward reaction will be favored, resulting in the formation of ZnO nuclei. On increasing growth duration the ZnO nuclei grow further to form ZnO nanoparticles (see Figure 2a). These nanoparticles grow broader and form

disc-like structures (see Figure 2b). This indicates that the initial growth unit is hexagonal discs. The ZnO crystal is polar in nature along the c-axis. The (001) plane is terminated by the Zn^{2+} ions while the (00-1) plane is O^{2-} ion terminated.

Table 1. Gibbs free energy of the compounds used in the reaction in the state of reaction [12].

Compound	State	ΔG (kJ/mol)
$Zn(CH_3(COO))_2$	Aqueous	–516.4
NaOH	Aqueous	–419.1
ZnO	Solid	–320.5
CH_3COONa	Aqueous	–631.2
H_2O	Liquid	–236.8

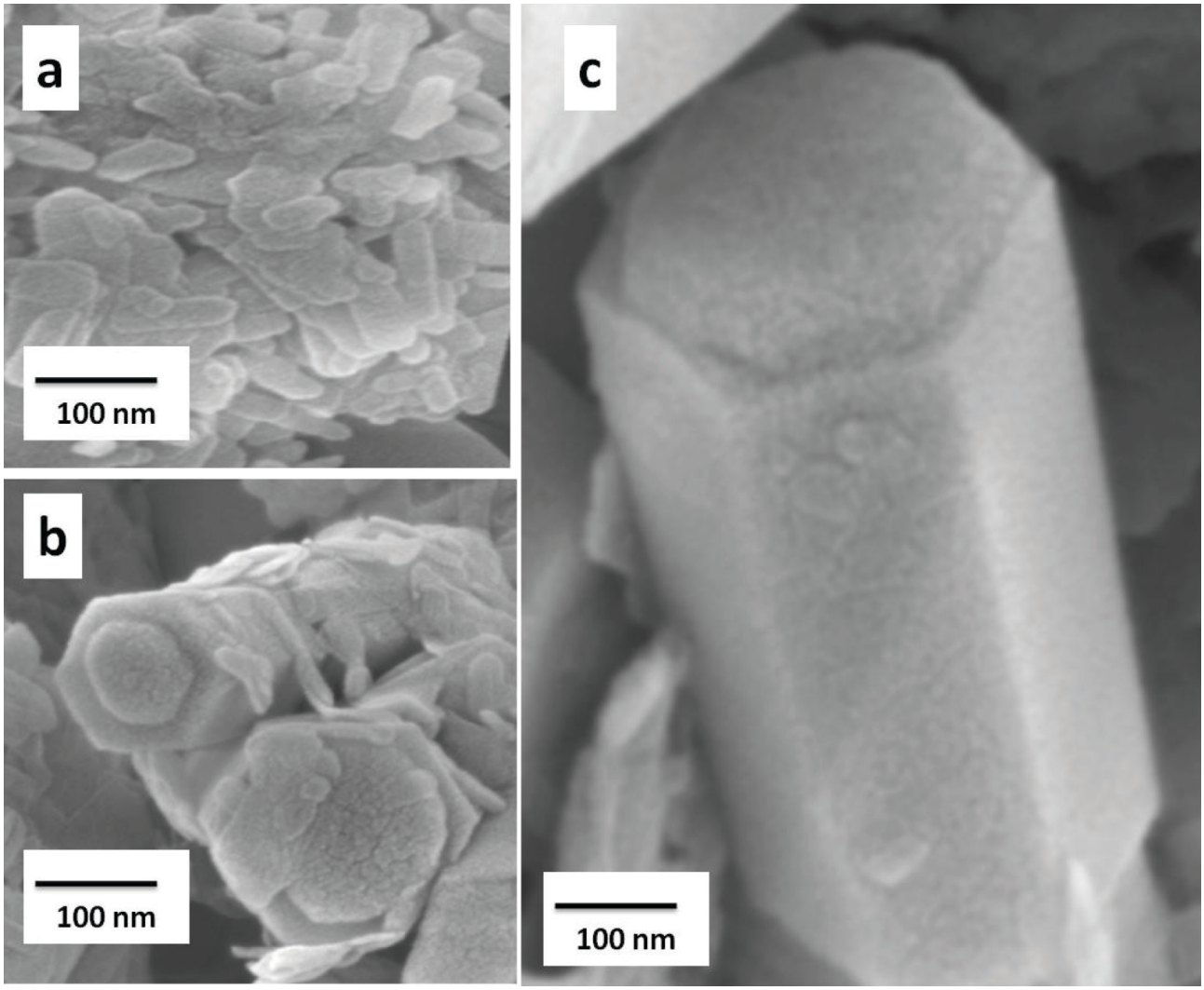

Figure 2. (a) Initially grown ZnO nanoparticles, (b) growth of ZnO nanodiscs, and (c) the grown ZnO nanorods.

Hence, due to further attachment of Zn^{2+} on the (001) plane and O^{2-} on the (00-1) plane, the disc-like structure extends along the c-axis and produces nanorods (see Figure 2c). In addition, the OH^- ions produced during decomposition of NaOH increase the pH of the solution and assist in further growth of the nanorods. Finally the growth of the nanorods saturates under the combined effect of ionic association/attachment of Zn^{2+} and OH^- ions, Gibbs free energy of the reaction, reaction temperature, and the enthalpy of the chemical system. On increasing the stirring further, dissolution occurs, leading to coarse edges on the top of the nanorods. On increasing the stirring, due to the high dissolution rate, the atoms in the core of the nanorods gradually vanish and finally hollow tubular structures are formed. Representative nanostructures grown in each step of this transformation are shown in Figures 3a–3c.

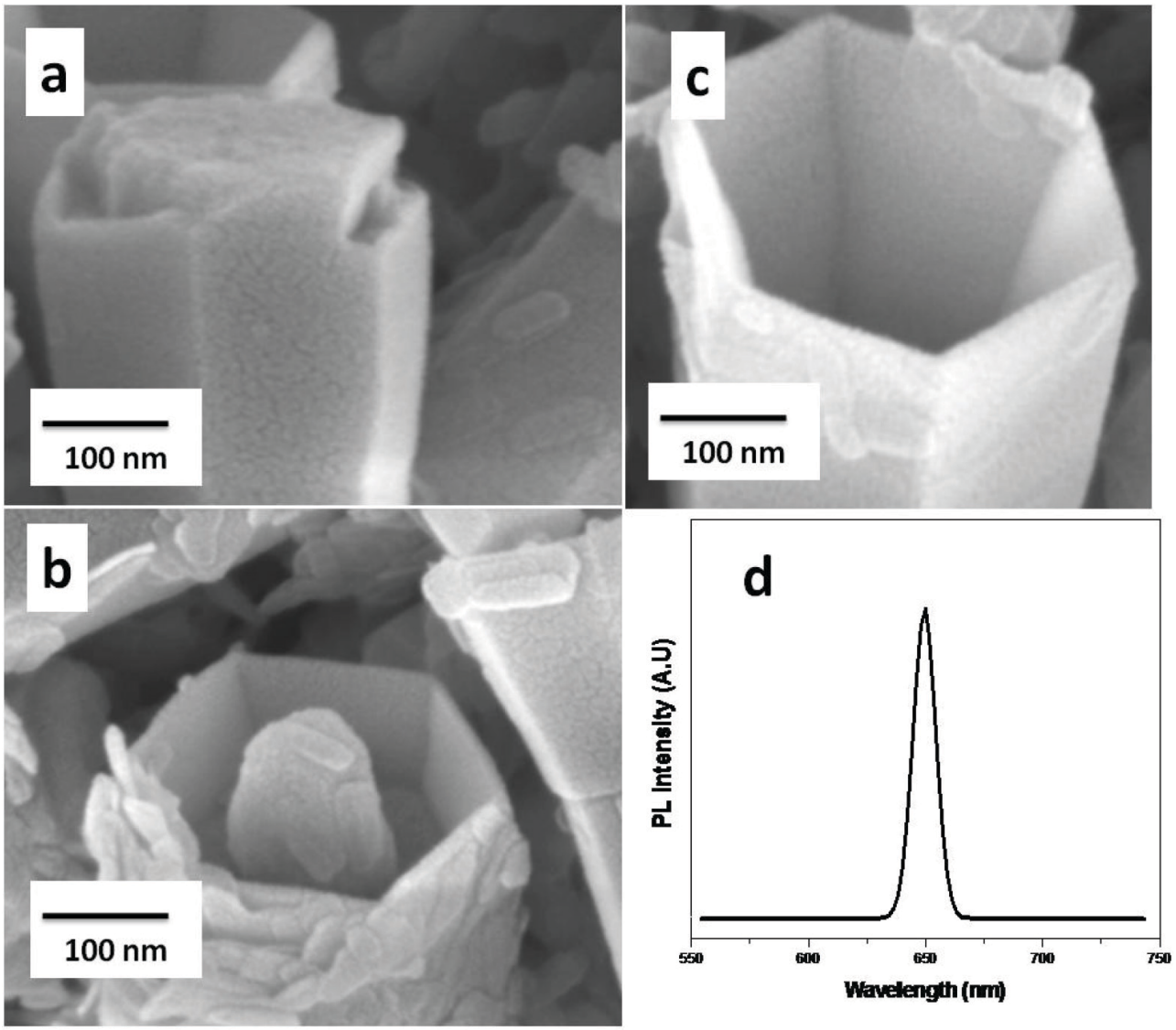

Figure 3. (a) Dissolution of atoms from ZnO nanorods, (b) high dissolution rates and wall thinning, (c) hollow ZnO nanotubes, (d) room temperature PL spectrum of ZnO nanotubes.

A typical room temperature PL spectrum of the ZnO nanotubes is shown in Figure 3d. A strong emission peak was observed at 649 nm. We used the full potential muffin-tin orbital model for defect states energy calculation of ZnO. It was found that this PL emission is due to the transitions of holes trapped at V_O^{++} states and the conduction band edge [13].

4. Conclusions

We reported the successful synthesis of ZnO nanorods and nanotubes of hexagonal surface structure. The growth of the nanorods was guided by the Gibbs free energy, precursors, and thermodynamics of the system. The nanorods were transformed to tubular structures due to dissolution of Zn and O atoms from the core of the nanorods. It was also observed that the dissolution was much more for longer duration of growth. This transformation of nanorods to nanotubes was also guided by the temperature of the solution, which needs further investigation.

References

[1] Zheng Z, Lin J, Song X, Lin Z. Optical properties of ZnO nanorod films prepared by CBD method. Chemical Physics Letters 2018; 712: 155-159. doi: 10.1016/j.cplett.2018.09.006

[2] Ta QTH, Namgung G, Noh J. Morphological evolution of solution-grown cobalt- doped ZnO nanostructures and their properties. Chemical Physics Letters 2018; 700: 1-6. doi: 10.1016/j.cplett.2018.04.002

[3] Wang Q, Qiu Y, Yang D, Li B, Zhang X et al. Improvement in piezoelectric performance of a ZnO nanogenerator by modulating interface engineering of CuO-ZnO heterojunction. Applied Physics Letters 2018; 113: 053901. doi: 10.1063/1.5035309

[4] Choi K, Chang S. Effect of structure morphologies on hydrogen gas sensing by ZnO nanotubes. Materials Letters 2018; 230: 48-52. doi: 10.1016/j.matlet.2018.07.031

[5] Carcia PF, McLean RS, Reilly MH, Nunes Jr G. Transparent ZnO thin-film transistor fabricated by rf magnetron sputtering. Applied Physics Letters 2003; 82 (7): 1117-1119. doi: 10.1063/1.1553997

[6] Yim K, Lee J, Lee D, Lee M, Cho E et al. Property database for single-element doping in ZnO obtained by automated first-principles calculations. Science Reports 2017; 7: 40907. doi: 10.1038/srep40907

[7] Ellmer K, Bikowski A. Intrinsic and extrinsic doping of ZnO and ZnO alloys. Journal of Physics D: Applied Physics 2016; 49: 413002. doi: 10.1088/0022-3727/49/41/413002

[8] Han S, Akhtar MS, Jung I, Yang O. ZnO nanoflakes nanomaterials via hydrothermal process for dye sensitized solar cells. Materials Letters 2018; 2309: 92-95. doi: 10.1016/j.matlet.2018.07.083

[9] Bueno C, Maestre D, Díaz T, Pacio M, Cremades A. Fabrication of ZnO-TiO_2 axial micro-heterostructures by a vapor-solid method. Materials Letters 2018; 220: 56-160. doi: 10.1016/j.matlet.2018.03.036

[10] Pyun YB, Yi J, Lee DH, Son KS, Liu G et al. Synthesis of ZnO nanotubes and nanotube-nanorod hybrid hexagonal networks using a hexagonally close-packed colloidal monolayer template. Journal of Material Chemistry 2010; 20: 5136-5140. doi: 10.1039/c0jm00011f

[11] Lide DR. Handbook of Chemistry and Physics. 85th ed. Boca Raton, FL, USA: CRC Press, 2005.

[12] Staemmler V, Fink K, Meyer B, Marx D, Kunat M et al. Stabilization of polar ZnO surfaces: validating microscopic models by using CO as a probe molecule. Physical Review Letters 2003; 90: 106102. doi: 10.1103/PhysRevLett.90.106102

[13] Kim Y, Park CH. Rich variety of defects in ZnO via an attractive interaction between O vacancies and Zn interstitials: origin of n-type doping. Physical Review Letters 2009; 102: 086403. doi: 10.1103/PhysRevLett.102.086403